RAPID COMMUNICATIONS

PHYSICAL REVIEW B **96**, 020101(R) (2017)

Accuracy of *GW* for calculating defect energy levels in solids

Wei Chen* and Alfredo Pasquarello

Chaire de Simulation à l'Echelle Atomique (CSEA), Ecole Polytechnique Fédérale de Lausanne (EPFL), CH-1015 Lausanne, Switzerland

(Received 21 May 2017; published 5 July 2017)

The accuracy of GW in the determination of defect energy levels is assessed through calculations on a set of well-characterized point defects in semiconductors: the As antisite in GaAs, the substitutional Mg in GaN, the interstitial C in Si, the Si dangling bond, and the Si split-vacancy complex in diamond. We show that the GW scheme achieves a reliable description of charge transition levels, but the overall accuracy is comparable to that of hybrid-functional calculations.

DOI: 10.1103/PhysRevB.96.020101

The electrical activity of point defects in semiconductors is associated with defect energy levels or, more specifically, charge transition levels between different charge states of the defect [1,2]. Defect energy levels are accessible by electrical and optical measurements, but the origin of the defect levels often remains obscure from experiment alone and needs to be addressed through first-principles calculations. While defect calculations within the framework of density functional theory (DFT) have grown into a well-established formulation, early practices of using semilocal density functionals have cast doubts on the reliability of the calculated defect levels due to the severe underestimation of the band gap. The true predictive power of first-principle calculations has emerged only recently as hybrid-functional calculations have become more affordable. Calculated defect energy levels generally agree well with experiment provided the experimental band gap is well reproduced by the hybrid functional.

Alternatively, many-body perturbation theory in the GW approximation represents a rigorous approach for the electronic-structure problem [3]. Combining the quasiparticle (QP) energies with DFT generated structures, the GW method is considered as the state-of-the-art approach for the calculation of defect energy levels overcoming the "band-gap problem" [4,5]. A full-fledged GW defect study comprises the polarizability and self-energy calculation of defect-containing supercells, thereby describing the QP energies of the defect and of the host band structure on an equal footing. As a result, GW defect calculations can be very demanding and are scarcely available in the literature (less than 20 papers) [4–21] because of the unfavorable quartic scaling with system size. In practice, the correlation part of the GW self-energy only contains the ring diagram of the random phase approximation (RPA), and is therefore not free from the self-interaction (or self-screening) error [9,22–26]. Indeed, studies on ionization potentials suggest that the GW approximation is not necessarily more accurate than (optimized) hybrid functionals for band-edge positions [25,27]. For defect energy levels, the limited number of GW calculations in the literature do not deliver a clear message concerning their accuracy since experimental references that could serve as benchmarks are often unavailable.

In this work, we focus on a series of experimentally well-characterized defects in semiconductors. The selected defects are technologically relevant, and consist of the As antisite in GaAs (As_{Ga}) [28], the substitutional Mg in GaN (Mg_{Ga}) [29–31], the interstitial C in Si (C_i) [32], the Si dangling bond (DB) [33], and the Si split-vacancy complex (SiV) in diamond [34,35]. The host materials exhibit band gaps ranging from 1.2 eV (Si) to 5.5 eV (diamond), and bonding characteristics from pure covalent (Si and diamond) to mixed ionic-covalent (GaAs and GaN) bond. The present study on defect levels allows us, on the one hand, to confront the performance of GW and hybrid-functional calculations, and, on the other hand, to assess their overall accuracy with respect to experiment.

For the GW calculation of defect levels, we follow the protocol outlined in Ref. [36]. In particular, the electrostatic finite-size effect in the one-particle energy level of charged defects and the path dependence of thermodynamic charge transition levels are taken into account. A $2 \times 2 \times 2$ Γ-centered Monkhorst-Pack **k**-point mesh [37] is used for the 64-atom cubic supercell (Si, C, and GaAs), whereas the sole Γ point is used for the 96-atom supercell of wurtzite GaN. The dielectric function is evaluated by the contour deformation method [38], including unoccupied states up to 80 eV above Fermi level in the summation. The GW QP energies are extrapolated to the infinite band limit based on the $1/N_b$ asymptotic behavior, where N_b is the number of bands included in the self-energy calculation. With the current computational setup, the reported QP energies are expected to be converged within 0.1 eV.

The GW calculations in this work correspond to one-shot G_0W_0 based on starting points obtained with the screened hybrid-functional proposed by Heyd-Scuseria-Ernzerhof (HSE06, hereafter denoted as HSE) [39]. For a suitable fraction of Fock exchange α in the hybrid-functional starting point, the band gap calculated at the G_0W_0 level can reproduce the experimental band gap, a prerequisite for a direct comparison between theoretical and experimental defect energy levels. Table I lists the optimal values of the parameter α for the four semiconductors under consideration in this work. Note that for Si and diamond, G_0W_0 on top of the semilocal Perdew-Burke-Ernzerhof (PBE) functional [40] already gives a band gap close to experiment [27]. Starting from HSE will inevitably lead to band gaps that are too large for these two materials. However, the use of the PBE starting point suffers from one critical issue: the one-particle Kohn-Sham eigenstates associated with the defect could erroneously fall in

*Present address: Institute of Condensed Matter and Nanosciences (ICMN), Université Catholique de Louvain, Louvain-la-Neuve 1348, Belgium; wei.chen@uclouvain.be

 ©2017 American Physical Society

TABLE I. Experimental lattice parameters a and c and fractions of Fock exchange α required to reproduce the experimental band gap E_g (at low temperature).

	a (c) (Å)	α (HSE)	α (G_0W_0@HSE)	E_g (eV)
GaAs	5.65[a]	0.30	0.25	1.5
GaN	3.19 (5.19)[a]	0.33	0.28	3.5
Si	5.43[b]	0.25	0.15[c]	1.2
C	3.57[b]	0.28	0.10[c]	5.5

[a]Reference [53].
[b]Reference [54].
[c]Vertex corrections are included in the screening W through the bootstrap exchange-correlation kernel.

the vicinity of the band edges, sometimes even merge into the valence or conduction band, hence sabotaging the screening and the final QP energies in the G_0W_0 calculations. HSE calculations generally do not suffer from such an issue as the calculated band gap is more realistic. On this account, we keep the HSE starting point for Si and C, but additionally include vertex corrections in the screened interaction W by using the bootstrap exchange-correlation kernel in the dielectric function [41,42]. In principle, vertex corrections can also be applied to GaAs and GaN, but their effect is marginal compared to the conventional RPA GW, once the same band gap is enforced through the use of an α-optimized starting point. To show this, we check the quasiparticle energies for the neutral $\mathrm{As_{Ga}}$ in GaAs and for the negatively charged $\mathrm{Mg_{Ga}}$ in GaN with vertex corrections in W taken into account. Consequently, the required α needs to be increased to 0.40 and 0.45 for GaAs and GaN, respectively, to ensure that the experimental band gap is reproduced. In both cases, we find that the defect levels shift by only 0.03 eV when referred to the band edges. Such a remarkable agreement between the two schemes further implies that the accuracy obtained in this work is characteristic of the GW approximation, and is largely irrespective of the specific starting point or of the adopted type of screening.

Defect structures are relaxed with the HSE hybrid functional. In these structural relaxations, the mixing parameters α are chosen so that the HSE functional used for the relaxation reproduces the experimental band gap. This leads to a different set of parameters α than used for the starting points of the G_0W_0 calculations (cf. Table I). Using the HSE functional with α determined in this way, we also extract the defect energy levels at the HSE level. The same **k**-point meshes as in the GW calculations are adopted. Hence, two advanced electronic structure methods, both reproducing the experimental band gap, are compared here with each other and with experiment. Finite-size corrections of total energies due to the spurious Coulomb interactions are applied to charged defects using the technique of Freysoldt *et al.* [43,44]. The latter corrections are fully consistent with the eigenvalue corrections applied in the GW calculations [17,36].

Incomplete structural relaxations arising from the long-range elastic interaction between defects [45] also need to be addressed. An earlier study showed that such effects amount to errors of less than 0.05 eV in the case of the $\mathrm{As_{Ga}}$ antisite when a 64-atom supercell is used (cf. Fig. 1 of Ref. [46]). Here, we assess the elastic effect at the PBE level by comparing charge transition levels calculated by varying the supercell size (up to 216 atoms). The error is typically smaller than 0.1 eV for defects in Si, but in the case of the SiV defect in diamond, we record residual errors up to 0.2 eV. Similarly, the single-particle energy level in the GW scheme is also subject to change in the dilute limit due to the elastic effect. Nonetheless, we find that the effect is generally small, about 0.1 eV or less when using the 64-atom supercell. Therefore, we include the elastic corrections neither in the GW nor in the hybrid calculations. This residual uncertainty should be borne in mind when comparing the calculated charge transition levels with experiment.

Throughout this work, we use the newly developed optimized norm-conserving Vanderbilt pseudopotentials (ONCVPSP) [47]. For Ga, $3s$, $3p$, $3d$, $4s$, and $4p$ electrons are included among the valence states. Due to the high computational cost of GW calculations, we slightly relax the cutoff radius of the Ga pseudopotential to lower the required plane-wave cutoff energy to 70 Ry. With this adjustment, the QP energies still agree within 0.05 eV compared to the standard dataset [48]. The GW calculations are performed using the code ABINIT [49]. The HSE structural relaxations and total-energy calculations are carried out with the code QUANTUM ESPRESSO [50] and are accelerated by the low-rank approximation of Fock exchange [51]. We use the experimental lattice parameters listed in Table I.

In Table II, the calculated charge transition levels are collected and compared to the experimental values. The latter are often measured through optical methods thus involving excitonic effects. Nevertheless, excitonic energies are very small for the present four semiconductors [52], and can thus safely be disregarded when comparing with theoretical values.

As_{Ga} in GaAs. The As antisite defect, i.e., an As atom occupying a Ga lattice site, is related to the important *EL*2 center, a double donor compensating shallow acceptors and pinning the Fermi level at midgap [63,64]. The microscopic structure of the *EL*2 center has been largely debated and has motivated extensive experimental and theoretical studies [65], but the isolated $\mathrm{As_{Ga}}$ defect of tetrahedral symmetry is now widely accepted [66,67]. A general consensus prevails about the experimental defect energy levels of $\mathrm{As_{Ga}}$. Electron paramagnetic resonance (EPR) measurements by Weber *et al.* identified two donor levels at $E_c - 0.75$ $(+/0)$ and $E_v + 0.5$ eV $(2+/+)$ [55], where E_v (E_c) denotes the valence-band (conduction-band) edge. Lagowski *et al.* reported two donor levels at $E_v + 0.54$ and $E_v + 0.77$ eV as measured with deep-level transient spectroscopy (DLTS) and photocapacitance spectroscopy at 77 K in p-type GaAs [28]. Identical levels were also found by Omling *et al.* with photocapacitance measurements in n-type samples [56]. The thermodynamic charge transition levels of $\mathrm{As_{Ga}}$ calculated at the GW level agree extremely well with the experimental levels (cf. Table II). A better accuracy is achieved than with HSE calculations, in particular for the upper $(+/0)$ level. We note that our calculations do not take into account spin-orbit coupling (SOC), which would make the GW calculations elusive. Charge transition levels have previously been shown not to be affected by SOC effects when aligned to the average electrostatic potential [46]. Nevertheless, SOC effects account

TABLE II. Thermodynamic charge transition levels referred to the valence-band maximum, as obtained through the GW and HSE calculations. Mean absolute error (MAE) and mean signed error (MSE) with respect to the experimental data are given. Results from previous hybrid-functional results are given for comparison. All energies are in eV.

	G_0W_0@HSE	HSE	Prev. hybrid	Expt.
As_{Ga} in GaAs				
(+/0)	0.8	1.0	0.97[a]	0.77[b]
(2+/+)	0.5	0.6	0.57[a]	0.54[b]
Mg_{Ga} in GaN				
(0/−)	0.6	0.4	0.26[c], 0.38[d]	0.225[e]
C_i in Si				
(+/0)	0.4	0.4	0.31[f]	0.28[g]
(0/−)	1.2	1.1	0.98[f]	1.10[g]
Si DB				
(+/0)	0.3	0.1	0.20[h]	0.26[i]
(0/−)	0.8	0.7	0.80[h]	0.84[i]
SiV in C				
(0/−)	1.9	1.6	1.43[j]	1.5[k]
MAE	0.14	0.12		
MSE	0.12	0.04		

[a]Reference [46], HSE06 ($\alpha = 0.35$).
[b]Reference [28], DLTS and photocapacitance measurement at 77 K. Similar results are obtained in Ref. [55] by EPR and in Ref. [56] by photocapacitance measurements.
[c]Reference [57], HSE06 ($\alpha = 0.31$).
[d]Reference [58], HSE06 ($\alpha = 0.31$).
[e]Reference [29–31], PL at 2 K.
[f]Reference [59], HSE06 ($\alpha = 0.25$).
[g]Reference [32], EPR and DLTS at room temperature.
[h]Reference [60], PBE0 ($\alpha = 0.10$).
[i]Reference [33], C-V measurements. Similar results are obtained by EPR and DLTS measurements in Ref. [61].
[j]Reference [62], HSE06 ($\alpha = 0.25$).
[k]Reference [34] (EPR, absorption, and photoluminescence at low temperature) and Ref. [35] (photoconductivity at 77 K).

for an upward shift of the valence-band maximum by ∼0.1 eV. Such a correction would retain the good agreement recorded for GW in Table II.

Mg_{Ga} in GaN. The substitutional Mg_{Ga} acceptor is so far the only effective acceptor for achieving p-type doping in GaN, and hence blue luminescence [68,69]. The Mg_{Ga} acceptor is at the origin of the 3.466 eV acceptor bound exciton accompanied by the 3.27 eV donor-acceptor pair peak found in the low-temperature photoluminescence (PL) spectra of Monemar *et al.* [29–31]. From this measurement, an acceptor binding energy of 225 meV can be inferred [29–31], which is in accord with an earlier estimate of 250 meV [70]. The signatures of the Mg acceptor have been identified consistently in a number of PL experiments [70]. The neutral Mg_{Ga}^0 defect shows C_{3v} symmetry. The Mg-N bond is stretched along the axial direction to accommodate the highly localized hole at the N site. The asymmetric distortion disappears in the negative charge state Mg_{Ga}^-. Consistently with previous hybrid-functional calculations [57,58], the present HSE calculations give the (0/−) charge transition level at 0.4 eV above E_v. On the other hand, the GW scheme yields a deeper acceptor level at $E_v + 0.6$ eV, thereby slightly worsening the agreement with experiment.

C_i in Si. The carbon interstitial (C_i) is commonly found in crystalline silicon upon radiation damage [71]. The configuration corresponds to a split Si-C interstitialcy defect along ⟨100⟩ with C_{2v} symmetry [32,71]. DLTS measurements by Song *et al.* identified the (+/0) single-donor level of the isolated C_i at $E_v + 0.28$ eV, and the (0/−) single-acceptor level at $E_c - 0.10$ eV [32]. We see in Table II that the DLTS defect levels are well reproduced by both HSE and GW calculations, with errors not exceeding ∼0.1 eV.

Si DB. This dangling bond (DB) defect refers to an unsaturated electron typically present at silicon interfaces or in amorphous silicon materials. The Si DB has been identified as the origin of the P_b center and gives rise to trap states at Si/SiO_2 interfaces [72], which are responsible for several device instabilities [73]. Poindexter *et al.* concluded that the Si DB defect is amphoteric and measured a (0/−) acceptor level at $E_v + 0.84$ (0.80) eV and a (+/0) donor level at $E_v + 0.26$ (0.31) eV through capacitance-voltage (C-V) and EPR measurements at Si(111)/SiO_2 interfaces [33]. DLTS experiments by Johnson *et al.* revealed a similar interface density profile showing a double peak at $E_c - 0.25$ and $E_v + 0.3$ eV for the acceptor and donor level, respectively [61]. Following Refs. [60,74], we model the Si DB by removing a cluster of four Si atoms in a Si supercell and passivating nine of the ten generated DBs by H atoms. Our HSE transition levels are about 0.1 eV lower compared to the experiment and to a previous calculation [60] based on the PBE0 hybrid functional [75]. The GW calculated acceptor ($E_v + 0.3$ eV) and donor ($E_v + 0.8$ eV) levels agree well with the experiments. It should be noted that our model does not properly account for the screening environment of Si DBs at the Si/SiO_2 interface. The effect of this limitation can be estimated by taking the Si DB in amorphous silicon under consideration. To a good approximation, the correlation energy U, i.e., the separation of the thermodynamic transition levels for (+/0) and (0/−), can be taken to be proportional to the inverse dielectric constant $1/\epsilon$ as it arises from electron-electron Coulomb interactions. For amorphous Si, estimates of 0.3 and 0.4 eV have been made for U [76], to be compared with the value of 0.5 eV at Si/SiO_2 interfaces. This leads us to conclude that the screening effect on the individual acceptor and donor levels should not exceed 0.1 eV.

SiV in C. The Si split-vacancy complex (SiV) is currently a heavily investigated color center in diamond for quantum optics and qubits, due to its bright and stable single-photon emission [77,78]. The SiV defect consists of an interstitial Si centered between two neighboring C vacancies along ⟨111⟩ with D_{3d} symmetry. The neutral SiV^0 is associated with a high-spin ground state ($S = 1$), in which the spin density is localized on four C dangling bonds in the double-degenerate e_g state [62,79]. The negatively charged SiV^- has a $S = 1/2$ ground state, and shows a slight Jahn-Teller distortion from D_{3d} symmetry [62]. EPR and PL studies have identified the SiV^0 and SiV^- defects as the origin of the zero-phonon lines (ZPLs) at 1.31 and 1.68 eV, respectively [34,77,79]. These transitions correspond to neutral excitations and are internal to defects in a specific charge state. Allers and Collins identified

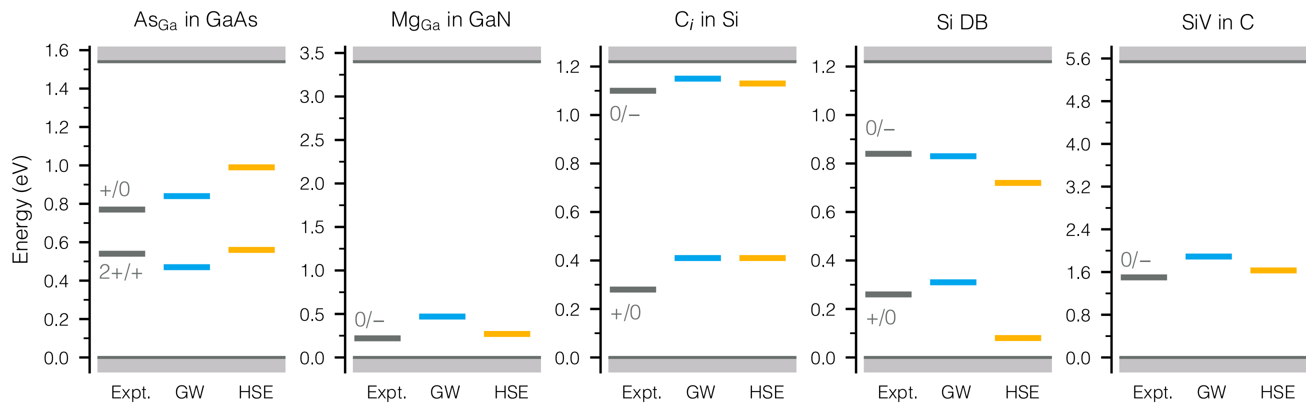

FIG. 1. Thermodynamic charge transition levels calculated with GW and HSE hybrid-functional calculations. The experimental reference levels are indicated.

a photoconductivity threshold at 1.5 eV in association with the 1.31 eV ZPL, but initially the origin of this feature could not be fully clarified [35]. D'Haenens-Johansson *et al.* recently concluded through a series of optical and EPR measurements that this transition is indeed related to the $(0/-)$ acceptor level [34]. In accord with Ref. [62], the present HSE calculations account well for the $(0/-)$ transition level. At variance, the GW calculations give rise to an acceptor level at $E_v + 1.9$ eV, lying ~ 0.4 eV deeper in the band gap compared to the experimental level.

For the present eight charge transition levels, the GW scheme achieves a satisfying overall accuracy as manifested by the mean absolute error (MAE) of 0.12 eV given in Table II. The HSE hybrid functional yields a similar MAE of 0.11 eV. These errors are of the same size as residual computational errors. The small difference between the GW and HSE scores therefore indicates that the accuracies of the two schemes should be considered as equivalent. Nevertheless, the HSE hybrid functional involves a considerably lower computational cost, and should therefore be preferred for the calculation of defect levels. Figure 1 shows that the GW calculations generally overestimate the defect energy levels, giving rise to a mean signed error (MSE) of about +0.1 eV (cf. Table II). For comparison, the MSE pertaining to HSE almost vanishes. In turn, this suggests that defect levels referred to the valence-band maximum lie systematically higher in GW than in HSE.

The systematic error inherent to the GW calculations should be associated to the "band-edge problem", awareness of which has lately been growing [17,80–85]. This occurs when the E_v levels as obtained with different theories are aligned differently with respect to the vacuum level or to the average electrostatic potential [80,81]. For the four semiconductors studied in this work, we find that E_v calculated at the GW level lies systematically deeper than the corresponding HSE level by 0.2–0.3 eV, when both schemes are aligned to the vacuum level and designed to reproduce the same experimental band gap. Indeed, irrespective of the starting point or the level of self-consistency, GW within the RPA tends to overestimate the ionization potentials of solids by similar amounts [25,27,86]. The downwards shift of E_v in the GW calculations leads to higher defect levels in the band gap, as the latter are more localized and therefore experience a weaker downwards shift than the delocalized band-edge levels [80,81].

In conclusion, our study shows that calculated defect levels referred to the valence-band edge can be obtained with an accuracy of about 0.1 eV on average, when using advanced electronic structure methods that have been empirically designed to reproduce the experimental band gap. GW and hybrid-functional calculations yield comparable accuracies. Our results hint at GW defect levels lying systematically at higher energies, possibly related to the general overestimation of GW ionization potentials seen previously [25,27,86]. Further work is necessary to investigate such effects in GW calculations.

This work is supported by the Swiss National Science Foundation (SNSF) under Grant No.200020-152799. Allocations of computational resources at Swiss National Supercomputing Center (CSCS) and SCITAS-EFPL are acknowledged.

[1] C. G. Van de Walle and J. Neugebauer, J. Appl. Phys. **95**, 3851 (2004).
[2] C. Freysoldt, B. Grabowski, T. Hickel, J. Neugebauer, G. Kresse, A. Janotti, and C. G. Van de Walle, Rev. Mod. Phys. **86**, 253 (2014).
[3] L. Hedin, Phys. Rev. **139**, A796 (1965).
[4] M. Hedström, A. Schindlmayr, G. Schwarz, and M. Scheffler, Phys. Rev. Lett. **97**, 226401 (2006).
[5] P. Rinke, A. Janotti, M. Scheffler, and C. G. Van de Walle, Phys. Rev. Lett. **102**, 026402 (2009).
[6] M. P. Surh, H. Chacham, and S. G. Louie, Phys. Rev. B **51**, 7464 (1995).
[7] M. L. Tiago and J. R. Chelikowsky, Phys. Rev. B **73**, 205334 (2006).
[8] Y. Ma and M. Rohlfing, Phys. Rev. B **77**, 115118 (2008).
[9] F. Bruneval, Phys. Rev. Lett. **103**, 176403 (2009).

[10] L. Martin-Samos, G. Roma, P. Rinke, and Y. Limoge, Phys. Rev. Lett. **104**, 075502 (2010).
[11] M. Bockstedte, A. Marini, O. Pankratov, and A. Rubio, Phys. Rev. Lett. **105**, 026401 (2010).
[12] S. Lany and A. Zunger, Phys. Rev. B **81**, 113201 (2010).
[13] F. Bruneval and G. Roma, Phys. Rev. B **83**, 144116 (2011).
[14] F. Bruneval, Nucl. Instrum. Methods Phys. Res. Sect. B **277**, 77 (2012).
[15] M. Jain, J. R. Chelikowsky, and S. G. Louie, Phys. Rev. Lett. **107**, 216803 (2011).
[16] P. Rinke, A. Schleife, E. Kioupakis, A. Janotti, C. Rödl, F. Bechstedt, M. Scheffler, and C. G. Van de Walle, Phys. Rev. Lett. **108**, 126404 (2012).
[17] W. Chen and A. Pasquarello, Phys. Rev. B **88**, 115104 (2013).
[18] A. Malashevich, M. Jain, and S. G. Louie, Phys. Rev. B **89**, 075205 (2014).
[19] F. Karsai, P. Tiwald, R. Laskowski, F. Tran, D. Koller, S. Gräfe, J. Burgdörfer, L. Wirtz, and P. Blaha, Phys. Rev. B **89**, 125429 (2014).
[20] M. Lorke, T. Frauenheim, and A. L. da Rosa, Phys. Rev. B **93**, 115132 (2016).
[21] M. A. Flores, W. Orellana, and E. Menéndez-Proupin, Phys. Rev. B **93**, 184103 (2016); Comput. Mater. Sci. **125**, 176 (2016).
[22] W. Nelson, P. Bokes, P. Rinke, and R. W. Godby, Phys. Rev. A **75**, 032505 (2007).
[23] P. Romaniello, S. Guyot, and L. Reining, J. Chem. Phys. **131**, 154111 (2009).
[24] F. Bruneval, J. Chem. Phys. **136**, 194107 (2012).
[25] A. Grüneis, G. Kresse, Y. Hinuma, and F. Oba, Phys. Rev. Lett. **112**, 096401 (2014).
[26] M. Dauth, F. Caruso, S. Kümmel, and P. Rinke, Phys. Rev. B **93**, 121115 (2016).
[27] W. Chen and A. Pasquarello, Phys. Rev. B **90**, 165133 (2014).
[28] J. Lagowski, D. G. Lin, T. Chen, M. Skowronski, and H. C. Gatos, Appl. Phys. Lett. **47**, 929 (1985).
[29] B. Monemar, P. P. Paskov, G. Pozina, C. Hemmingsson, J. P. Bergman, T. Kawashima, H. Amano, I. Akasaki, T. Paskova, S. Figge, D. Hommel, and A. Usui, Phys. Rev. Lett. **102**, 235501 (2009).
[30] B. Monemar, P. P. Paskov, G. Pozina, C. Hemmingsson, J. P. Bergman, H. Amano, I. Akasaki, S. Figge, D. Hommel, T. Paskova, and A. Usui, Phys. Status Solidi C **7**, 1850 (2010).
[31] B. Monemar, P. P. Paskov, G. Pozina, C. Hemmingsson, J. P. Bergman, S. Khromov, V. N. Izyumskaya, V. Avrutin, X. Li, H. Morkoç, H. Amano, M. Iwaya, and I. Akasaki, J. Appl. Phys. **115**, 053507 (2014).
[32] L. W. Song and G. D. Watkins, Phys. Rev. B **42**, 5759 (1990).
[33] E. H. Poindexter, G. J. Gerardi, M.-E. Rueckel, P. J. Caplan, N. M. Johnson, and D. K. Biegelsen, J. Appl. Phys. **56**, 2844 (1984).
[34] U. F. S. D'Haenens-Johansson, A. M. Edmonds, B. L. Green, M. E. Newton, G. Davies, P. M. Martineau, R. U. A. Khan, and D. J. Twitchen, Phys. Rev. B **84**, 245208 (2011).
[35] L. Allers and A. T. Collins, J. Appl. Phys. **77**, 3879 (1995).
[36] W. Chen and A. Pasquarello, J. Phys. Condens. Matter **27**, 133202 (2015).
[37] H. J. Monkhorst and J. D. Pack, Phys. Rev. B **13**, 5188 (1976).
[38] S. Lebègue, B. Arnaud, M. Alouani, and P. E. Bloechl, Phys. Rev. B **67**, 155208 (2003).
[39] J. Heyd, G. E. Scuseria, and M. Ernzerhof, J. Chem. Phys. **118**, 8207 (2003); **124**, 219906 (2006).
[40] J. P. Perdew, K. Burke, and M. Ernzerhof, Phys. Rev. Lett. **77**, 3865 (1996).
[41] S. Sharma, J. K. Dewhurst, A. Sanna, and E. K. U. Gross, Phys. Rev. Lett. **107**, 186401 (2011).
[42] W. Chen and A. Pasquarello, Phys. Rev. B **92**, 041115 (2015).
[43] C. Freysoldt, J. Neugebauer, and C. G. Van de Walle, Phys. Rev. Lett. **102**, 016402 (2009).
[44] H.-P. Komsa, T. T. Rantala, and A. Pasquarello, Phys. Rev. B **86**, 045112 (2012).
[45] C. Teodosiu, The elastic field of point defects, in *Elastic Models of Crystal Defects* (Springer, Berlin, 1982), pp. 287–316.
[46] H.-P. Komsa and A. Pasquarello, Phys. Rev. B **84**, 075207 (2011).
[47] D. R. Hamann, Phys. Rev. B **88**, 085117 (2013).
[48] The standard ONCVPSP-PBE-PDv0.3 dataset is available at https://github.com/abinit/pseudo_dojo
[49] X. Gonze, F. Jollet, F. A. Araujo, D. Adams, B. Amadon, T. Applencourt, C. Audouze, J.-M. Beuken, J. Bieder, A. Bokhanchuk, E. Bousquet, F. Bruneval, D. Caliste, M. Côté, F. Dahm, F. D. Pieve, M. Delaveau, M. D. Gennaro, B. Dorado, C. Espejo, G. Geneste, L. Genovese, A. Gerossier, M. Giantomassi, Y. Gillet, D. Hamann, L. He, G. Jomard, J. L. Janssen, S. L. Roux, A. Levitt, A. Lherbier, F. Liu, I. Lukačević, A. Martin, C. Martins, M. Oliveira, S. Poncé, Y. Pouillon, T. Rangel, G.-M. Rignanese, A. Romero, B. Rousseau, O. Rubel, A. Shukri, M. Stankovski, M. Torrent, M. V. Setten, B. V. Troeye, M. Verstraete, D. Waroquiers, J. Wiktor, B. Xu, A. Zhou, and J. Zwanziger, Comput. Phys. Commun. **205**, 106 (2016).
[50] P. Giannozzi, S. Baroni, N. Bonini, M. Calandra, R. Car, C. Cavazzoni, D. Ceresoli, G. L. Chiarotti, M. Cococcioni, I. Dabo, A. Dal Corso, S. de Gironcoli, S. Fabris, G. Fratesi, R. Gebauer, U. Gerstmann, C. Gougoussis, A. Kokalj, M. Lazzeri, L. Martin-Samos, N. Marzari, F. Mauri, R. Mazzarello, S. Paolini, A. Pasquarello, L. Paulatto, C. Sbraccia, S. Scandolo, G. Sclauzero, A. P. Seitsonen, A. Smogunov, P. Umari, and R. M. Wentzcovitch, J. Phys. Condens. Matter **21**, 395502 (2009).
[51] L. Lin, J. Chem. Theory Comput. **12**, 2242 (2016).
[52] *Group IV Elements, IV-IV and III-V Compounds. Part B - Electronic, Transport, Optical and Other Properties*, edited by O. Madelung, U. Rössler, and M. Schulz (Springer, 2002).
[53] I. Vurgaftman, J. R. Meyer, and L. R. Ram-Mohan, J. Appl. Phys. **89**, 5815 (2001).
[54] W. Parrish, Acta Crystallogr. **13**, 838 (1960).
[55] E. R. Weber, H. Ennen, U. Kaufmann, J. Windscheif, J. Schneider, and T. Wosinski, J. Appl. Phys. **53**, 6140 (1982).
[56] P. Omling, P. Silverberg, and L. Samuelson, Phys. Rev. B **38**, 3606 (1988).
[57] J. L. Lyons, A. Janotti, and C. G. Van de Walle, Phys. Rev. Lett. **108**, 156403 (2012).
[58] G. Miceli and A. Pasquarello, Phys. Rev. B **93**, 165207 (2016).
[59] P. Deák, B. Aradi, T. Frauenheim, E. Janzén, and A. Gali, Phys. Rev. B **81**, 153203 (2010).
[60] P. Broqvist, A. Alkauskas, and A. Pasquarello, Phys. Rev. B **78**, 075203 (2008).
[61] N. M. Johnson, D. K. Biegelsen, M. D. Moyer, S. T. Chang, E. H. Poindexter, and P. J. Caplan, Appl. Phys. Lett. **43**, 563 (1983).
[62] A. Gali and J. R. Maze, Phys. Rev. B **88**, 235205 (2013).

[63] W. E. Spicer, I. Lindau, P. Skeath, and C. Y. Su, J. Vac. Sci. Technol. **17**, 1019 (1980).
[64] D. Colleoni, G. Miceli, and A. Pasquarello, J. Phys.: Condens. Matter **26**, 492202 (2014).
[65] F. Koschnick and J.-M. Spaeth, Phys. Status Solidi B **216**, 817 (1999).
[66] J. Dabrowski and M. Scheffler, Phys. Rev. B **40**, 10391 (1989).
[67] H. Overhof and J.-M. Spaeth, Phys. Rev. B **72**, 115205 (2005).
[68] H. Amano, M. Kito, K. Hiramatsu, and I. Akasaki, Jap. J. App. Phys. **28**, L2112 (1989).
[69] S. Nakamura, T. Mukai, and M. Senoh, Appl. Phys. Lett. **64**, 1687 (1994).
[70] S. Strite and H. Morkoç, J. Vac. Sci. Technol. B **10**, 1237 (1992).
[71] G. D. Watkins and K. L. Brower, Phys. Rev. Lett. **36**, 1329 (1976).
[72] P. J. Caplan, E. H. Poindexter, B. E. Deal, and R. R. Razouk, J. Appl. Phys. **50**, 5847 (1979).
[73] P. M. Lenahan and J. F. Conley, Jr., J. Vac. Sci. Technol. B **16**, 2134 (1998).
[74] J. R. Weber, A. Janotti, P. Rinke, and C. G. Van de Walle, Appl. Phys. Lett. **91**, 142101 (2007).
[75] J. P. Perdew, M. Ernzerhof, and K. Burke, J. Chem. Phys. **105**, 9982 (1996).
[76] H. M. Branz, Phys. Rev. B **39**, 5107 (1989).
[77] T. Müller, C. Hepp, B. Pingault, E. Neu, S. Gsell, M. Schreck, H. Sternschulte, D. Steinmüller-Nethl, C. Becher, and M. Atatüre, Nat. Commun. **5**, 3328 (2014).
[78] K. D. Jahnke, A. Sipahigil, J. M. Binder, M. W. Doherty, M. Metsch, L. J. Rogers, N. B. Manson, M. D. Lukin, and F. Jelezko, New J. Phys. **17**, 043011 (2015).
[79] A. M. Edmonds, M. E. Newton, P. M. Martineau, D. J. Twitchen, and S. D. Williams, Phys. Rev. B **77**, 245205 (2008).
[80] A. Alkauskas, P. Broqvist, and A. Pasquarello, Phys. Rev. Lett. **101**, 046405 (2008).
[81] A. Alkauskas and A. Pasquarello, Phys. Rev. B **84**, 125206 (2011).
[82] A. Alkauskas, P. Broqvist, and A. Pasquarello, Phys. Status Solidi B **248**, 775 (2011).
[83] H. Peng, D. O. Scanlon, V. Stevanovic, J. Vidal, G. W. Watson, and S. Lany, Phys. Rev. B **88**, 115201 (2013).
[84] C. Freysoldt, B. Lange, J. Neugebauer, Q. Yan, J. L. Lyons, A. Janotti, and C. G. Van de Walle, Phys. Rev. B **93**, 165206 (2016).
[85] J. L. Lyons and C. G. Van de Walle, npj Comput. Mater. **3**, 1 (2017).
[86] Y. Hinuma, A. Grüneis, G. Kresse, and F. Oba, Phys. Rev. B **90**, 155405 (2014).